Progress In Electromagnetics Research, *PIER 31, 1–30, 2001*

FINITE DIFFERENCE TIME DOMAIN (FDTD) IMPEDANCE BOUNDARY CONDITION FOR THIN FINITE CONDUCTING SHEETS

J. J. Akerson

United States Air Force Academy
USAF Academy, CO 80840, USA

M. A. Tassoudji

QUALCOMM Incorporated
San Diego, CA 92121, USA

Y. E. Yang *

Rannoch Corporation
Cambridge, MA 02142, USA

J. A. Kong

Massachusetts Institute of Technology
Cambridge, MA 02139, USA

Abstract–A new Impedance Boundary Condition (IBC) for two dimensional Finite Difference Time Domain simulations containing thin, good conductor sheets is presented. The IBC uses a recursive convolution scheme based on approximating the conductor's impedance as a sum of exponentials. The effects of FDTD parameters such as grid size and time step on simulation accuracy are presented. The IBC verification is performed by comparing the quality factors of rectangular resonant structures determined by the FDTD simulation and analytical methods. The IBC is shown to accurately model the conductor loss over a wide frequency range.

* on leave from Massachusetts Institute of Technology, Cambridge, MA 02139, USA

1. INTRODUCTION

In Finite Difference Time Domain (FDTD) simulations involving highly conductive materials, such as the metal case of a computer system, the tangential electric fields are typically set to zero on the surface of the material. This Perfect Electric Conductor (PEC) assumption ignores any loss associated with the finite conductivity. The errors that result from this approximation should be weighed against the large cost of discretizing the lossy material. Since the wavelength of a highly conductive material is very small, in order to capture the loss mechanism within the conductor the simulation volume must be divided into a very fine grid. When the *brute force* method is used, computer resources are wasted by having to finely divide the the other less dense materials (e.g., free space). In these materials the fine grid is not necessary to capture the physics of the problem. The computational size can be reduced with a sub-gridding scheme where the conducting material uses much smaller grid than the rest of the computational domain[1–3]. For very good conductors; however, the grid size is so small that even sub-gridding is not a viable option. To overcome the resource problem, the surface of the highly conductive material can be replaced

with an Impedance Boundary Condition (IBC) [4–7]. An IBC is only appropriate when the simulation volume of interest is on one side of the conductive material. However, IBCs have the added complication that they are usually frequency dependent and are not directly useable to the the standard frequency independent FDTD equations. In this case the FDTD equations must be modified to incorporate the dispersive nature of the surface as in [8]. Typical frequency domain equations relating the electric fields and magnetic fields become convolution equations in time. Convolutions have a large computational and memory overhead, but if the convolution integral can be approximated by a sum of exponentials then recursive convolution can be implemented and the memory requirements reduced.

An FDTD formulation of finite conductivity has been used for modeling a good conductor [9]. This "synthetic" conductivity is derived by comparing the numerical impedance of the difference equations and the actual impedance of a good conductor at specified frequency. In this way the derived synthetic conductivity is inserted into the FDTD equations at the boundary only; thus being a surface boundary condition similar to an IBC. The advantage to this method is that no *new* equations are needed; however, its major disadvantage is that it is good at a single frequency.

An impedance boundary condition that incorporates the frequency dependence was developed for thin dielectric coatings over PEC surfaces [10]. The IBC starts with the analytically derived expression for the impedance in the frequency domain. The expression is expanded in a Taylor series about the wave number, k, and transformed to the time domain. The resulting partial differential equation is fourth order in time and first order in space. The difference equations do model the frequency characteristics fairly well; however, the equations are quite complicated and rely on many past values of the surface electric field. Furthermore, the condition is good at normal incidence only thus limited to 1D structures. This work is extended to include non-normal incidence [11]; however, the modified IBC is only good for a single incidence angle.

Like the IBC of [10], we start with a frequency domain expression for the impedance. This time for a thin sheet of a very good conductor. The frequency domain equation is transformed to the Laplace domain and the subsequent expression is approximated by a sum of first-order rational functions. This approximation is critical to the IBC's use-

fulness in FDTD simulations. The first-order rational functions are exponentials in time and thus a recursive convolution scheme is implemented. The benefit of this scheme is that it is good over a wide range of frequencies.

The same approach was applied to lossy dielectric portions of a FDTD computational domain with an IBC where the frequency domain impedance expression was approximated by a rational function using *Mathematica* and then expanded using partial fraction expansion [7].

This article describes the 1D Impedance Boundary Condition for thin finite conducting sheets and recursive convolution. Then the accuracy of the 1D IBC is examined and quantified. Finally, the IBC is extended to two dimensions and validated through the measurements of the *quality* factor of rectangular resonant cavities at different frequencies and conductivity values.

2. DERIVATION OF IMPEDANCE BOUNDARY CONDITION

To construct an impedance boundary condition we start with the impedance equation that relates the tangential components of the electric and magnetic field at an interface between two different media,

$$\bar{E}_{\tan}(\omega) = Z(\omega)\left[\hat{n} \times \bar{H}_{\tan}(\omega)\right], \tag{1}$$

where $\bar{E}_{\tan}$ and $\bar{H}_{\tan}$ are the tangential components of the electric and magnetic fields and $\hat{n}$ is the normal unit vector pointing out at the interface. For a conducting media characterized by permittivity, ϵ, permeability, μ_o, and conductivity, σ. If the media is a *good* conductor such that $1 \ll \frac{\sigma}{\omega\epsilon}$ then the permittivity of the conductor can be approximated by

$$\epsilon_c \approx i\frac{\sigma}{\omega}. \tag{2}$$

In one dimensional simulations (Figure 1), since propagation is normal to the surface, the surface impedance of a thin good conductor can be modeled as a transmission line with thickness l and characteristic impedance of a transmission line $\eta_c = \sqrt{\frac{\mu_o}{\varepsilon_c}}$. From transmission line theory, if a transmission line is terminated with impedance η_t then the impedance seen at distance l from the termination is

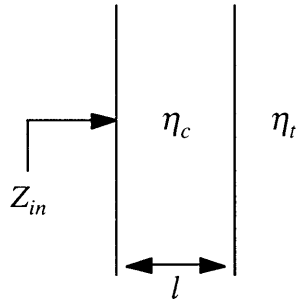

Figure 1. 1D transmission line model used for IBC formulation.

$$Z_{in} = \eta_c \frac{\eta_t - \eta_c \tanh(ik_c l)}{\eta_c - \eta_t \tanh(ik_c l)}. \tag{3}$$

When the termination impedance is free space i.e., $\eta_t = \eta_o \gg \eta_c$, then input impedance can be approximated by

$$Z_{in} \approx \eta_c \coth(ik_c l). \tag{4}$$

To make it easier to turn the boundary condition into time domain equations, it is useful to rewrite it in the Laplace domain form. The Laplace transform of (4) is

$$Z_{in}(s) = \sqrt{\frac{\mu_o s}{\sigma}} \coth\left(\sqrt{\frac{\mu_o s}{\sigma}}\sigma l\right). \tag{5}$$

Using power series expansions for cosh and sinh [12],

$$\cosh z = \prod_{k=1}^{\infty}\left[1 + \frac{4z^2}{(2k-1)^2\pi^2}\right] \tag{6}$$

and

$$\sinh z = z\prod_{k=1}^{\infty}\left[1 + \frac{z^2}{k^2\pi^2}\right], \tag{7}$$

the input impedance (5) can be represented by a quotient of two infinite products:

$$Z_{in}(s) = \frac{1}{\sigma l}\frac{\prod_{m=1}^{\infty}\left[1 + \frac{4\mu_o\sigma l^2}{(2m-1)^2\pi^2}s\right]}{\prod_{m=1}^{\infty}\left[1 + \frac{\mu_o\sigma l^2}{m^2\pi^2}s\right]}. \tag{8}$$

To use this relationship within the FDTD framework the impedance condition (1) must be transformed into the time domain,

$$\bar{E}_{\tan}(t) = \int_0^t Z(t-\tau)\left[\hat{n} \times \bar{H}_{\tan}(\tau)\right] d\tau. \tag{9}$$

A simple expression for $\bar{E}_{\tan}(t)$ must be found that can be converted to update equations that do not explicitly use the convolution integral of (9). This can be accomplished by approximating (8) with P terms in the denominator and $P-1$ terms in the numerator. The quotient can be expressed as a sum of quotients using partial fraction expansion and then transformed into the time domain. The result is a sum of exponentials,

$$Z(t) \approx \sum_{m=1}^{P} C_m e^{A_m t}, \tag{10}$$

where A_m is the mth pole and C_m in the mth residue of (8), given by

$$A_m = -\frac{m^2\pi^2}{\mu_o \sigma l^2} \tag{11}$$

and

$$C_m = \left(1 + \frac{\mu_o \sigma l^2}{m^2\pi^2} s\right) Z_{in}(s)\Big|_{s=A_m}. \tag{12}$$

3. RECURSIVE CONVOLUTION

Recursive convolution is possible when one of the operands is an exponential function. Since we have expressed the impedance of (9) as a sum of exponentials recursive convolution can be used. As in [7], we begin with the following convolution integral,

$$y(t) = \int_0^t a e^{-b(t-\tau)} x(\tau) d\tau, \tag{13}$$

and discretize it so that

$$y(n\Delta t) = \sum_{k=0}^{n-1} \int_{k\Delta t}^{(k+1)\Delta t} a e^{-b(n\Delta t - \tau)} x(\tau) d\tau. \tag{14}$$

Assuming that $x(t)$ is constant over the interval (i.e., piecewise constant), the integration over τ yields

$$y(n\Delta t) = \frac{a}{b}\sum_{k=0}^{n-1} x(k\Delta t)e^{-b(n-k)\Delta t}(e^{b\Delta t}-1). \tag{15}$$

Remove the n th term from the summation,

$$y(n\Delta t) = \frac{a}{b}\sum_{k=0}^{n-2} x(k\Delta t)e^{-b(n-k)\Delta t}(e^{b\Delta t}-1) + \frac{a}{b}x(k\Delta t)e^{-b\Delta t}(e^{b\Delta t}-1), \tag{16}$$

and rewrite the sum over $n-2$ so that

$$\begin{aligned}\sum_{k=0}^{n-2} x(k\Delta t)e^{-b(n-k)\Delta t}(e^{b\Delta t}-1) &= \sum_{k=0}^{n-2} x(k\Delta t)e^{-b(n-k-1)\Delta t}e^{-b\Delta t}(e^{b\Delta t}-1)\\ &= e^{-b\Delta t}\sum_{k=0}^{n-2} x(k\Delta t)e^{-b(n-k-1)\Delta t}(e^{b\Delta t}-1)\\ &= e^{-b\Delta t}y((n-1)\Delta t).\end{aligned} \tag{17}$$

The result is the basis for a recursive convolution equation:

$$y(n\Delta t) = e^{-b\Delta t}y((n-1)\Delta t) + \frac{a}{b}x((n-1)\Delta t)(1-e^{-b\Delta t}). \tag{18}$$

In the derivation above we assume $x(t)$ could be approximated as $x(n\Delta t)$ over the interval $[n\Delta t,(n+1)\Delta t]$. If we assume a piecewise linear approximation instead of piecewise constant, $x(t)$ is approximated as

$$x(t) \simeq x(n\Delta t) + \frac{t}{\Delta t}(x((n+1)\Delta t) - x(n\Delta t)) \tag{19}$$

so that

$$\begin{aligned}y(n\Delta t) = \sum_{k=0}^{n-1}\int_{k\Delta t}^{(k+1)\Delta t} & ae^{-b(n\Delta t-\tau)}\\ &\cdot\left[x(n\Delta t) + \frac{\tau-k\Delta t}{\Delta t}(x((n+1)\Delta t)-x(n\Delta t))\right]d\tau\end{aligned} \tag{20}$$

and the recursion formula becomes

$$y(n\Delta t) = e^{-b\Delta t}y((n-1)\Delta t) + \frac{a}{b}\Bigg\{x(n\Delta t)\left[1+\frac{1}{\Delta t b}(e^{-b\Delta t}-1)\right] + x((n-1)\Delta t)\left[\frac{1}{\Delta t b} - e^{-b\Delta t}(1+\frac{1}{\Delta t b})\right]\Bigg\}. \tag{21}$$

4. IMPLEMENTATION OF IMPEDANCE BOUNDARY CONDITION IN FDTD

Now that we have the form of the recursive convolution integrals we can construct FDTD IBC update equations.

4.1 Impedance Equations — Piecewise Constant Assumption

The derivation of the previous section can be used to construct the FDTD update equations if we let

$$y(n\Delta t) \rightarrow \bar{G}_m^n, \tag{22}$$

$$x((n-1)\Delta t) \rightarrow \hat{n} \times \bar{H}_{tan}^{n-\frac{1}{2}}, \tag{23}$$

and

$$ae^{-bn\Delta t} \rightarrow C_m e^{A_m n\Delta t}. \tag{24}$$

Substitution into (19) gives

$$\bar{G}_m^n = \bar{G}_m^{n-1}e^{A_m\Delta t} + \left(\hat{n}\times\bar{H}_{tan}^{n-\frac{1}{2}}\right)\frac{C_m}{A_m}\left(e^{A_m\Delta t}-1\right) \tag{25}$$

The tangential electric field update equation at the conductor surface is

$$\bar{E}_{tan}^n = \sum_{m=1}^{P}\bar{G}_m^n \tag{26}$$

The impedance equation relates the electric and magnetic fields at the same position and at the same time. However, in this work, we use the tangential electric field on the surface accompanied by the tangential

magnetic field half a grid space away and we take a time average of the electric field so that the update equation becomes

$$\bar{E}_{tan}^{n} = -\bar{E}_{tan}^{n-1} + 2\sum_{m=1}^{P} G_m^{n-\frac{1}{2}}. \tag{27}$$

The tangential electric field on the surface at the current time step, n, is a function of last tangential electric field and the last sum, $\bar{G}_m$. Compared to the full convolution, memory requirements are low since this method requires only $2P$ variables for the poles and residues and P variables for each grid point on the surface containing a tangential electric field.

4.2 Impedance Equations — Piecewise Linear Assumption

When more accuracy is desired the piecewise linear assumption can be used so that the tangential electric field's update equation is still (27) but now

$$\begin{aligned} \bar{G}_m^n = {} & \bar{G}_m^{n-1} e^{A_m \Delta t} \\ & + \left(\hat{n} \times \bar{H}_{tan}^{n-\frac{1}{2}}\right) \frac{C_m}{A_m} \left[\frac{1}{A_m \Delta t}\left(e^{A_m \Delta t} - 1\right) - 1\right] \\ & + \left(\hat{n} \times \bar{H}_{tan}^{n-\frac{3}{2}}\right) \frac{C_m}{A_m} \left[\frac{1}{A_m \Delta t} + e^{A_m \Delta t}\left(1 - \frac{1}{A_m \Delta t}\right)\right]. \end{aligned} \tag{28}$$

Improved accuracy is obtained at the expense of a more complicated equation and an additional memory location for each tangential electric field component on the surface.

5. EXTENSION OF IBC TO TWO DIMENSIONS

The use of the transmission line to model the impedance of a thin finite conducting sheet is completely justified in 1D simulations since propagation is fixed in the normal direction. On the other hand, since the the angle of incidence is not restricted to normal incidence in 2D simulations, we must verify that the model is still valid.

Consider phase matching at the surface of the conductor, located at $z = 0$, where k_i is the wave number on the free space side with incidence angle θ_i and k_c is the wave number in the conductor with a transmission angle of θ_c. The incident components of the k vector

are $k_{ix} = k_0 \sin\theta_i$ and $k_{iz} = k_0 \cos\theta_i$ and the conductor wave number is $k_c = k_0\sqrt{1 + i\frac{\sigma}{\omega\epsilon_0}}$.

Since phase matching says $k_{ix} = k_{cx}$, we know $k_{cz}^2 = k_c^2 - k_{ix}^2$. Solving for k_{cz},

$$k_{cz}^2 = k_0^2 \left(\cos\theta_i{}^2 + i\frac{\sigma}{\omega\epsilon_0} \right), \tag{29}$$

and using the good conductor approximation, we find

$$k_{cz} \simeq k_0\sqrt{\frac{\sigma}{2\omega\epsilon_0}}(1+i). \tag{30}$$

The angle in the conductor is given by

$$\tan\theta_c = \frac{k_{cx}}{\mathrm{Re}\{k_{cz}\}} = \sin\theta_i\sqrt{\frac{2\omega\epsilon_0}{\sigma}}. \tag{31}$$

Since $\sqrt{\frac{\sigma}{\omega\epsilon_0}}$ is very large, the propagation direction will, for all practical purposes, be normal to the surface regardless of the incidence angle. Therefore, we expect the transmission line model to apply even in the two dimensional case.

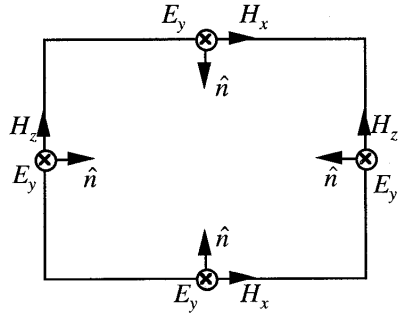

Figure 2. 2D configuration used for IBC equations of a rectangular resonator.

Figure 2 is a schematic of a 2D rectangular resonator with finite conducting walls. The relationships between the tangential electric and magnetic walls and the surface normal are shown and are used to construct IBC equations for each of the four walls. If the computational

domain is $N_x \times N_z$, the piecewise constant equations are

$$E_y^n(0,k) = -E_y^{n-1}(0,k) + 2\sum_{m=1}^{P}\left[G_m^{n-1}e^{A_m\Delta t} - H_z^{n-\frac{1}{2}}\left(\frac{1}{2},k\right)\frac{C_m}{A_m}(e^{A_m\Delta t}-1)\right], \quad (32)$$

for the left wall;

$$E_y^n(N_x,k) = -E_y^{n-1}(N_x,k) + 2\sum_{m=1}^{P}\left[G_m^{n-1}e^{A_m\Delta t} + H_z^{n-\frac{1}{2}}\left(N_x-\frac{1}{2},k\right)\frac{C_m}{A_m}(e^{A_m\Delta t}-1)\right], \quad (33)$$

for the right wall;

$$E_y^n(i,0) = -E_y^{n-1}(0,k) + 2\sum_{m=1}^{P}\left[G_m^{n-1}e^{A_m\Delta t} + H_x^{n-\frac{1}{2}}\left(i,\frac{1}{2}\right)\frac{C_m}{A_m}(e^{A_m\Delta t}-1)\right], \quad (34)$$

for the lower wall; and

$$E_y^n(i,N_z) = -E_y^{n-1}(i,N_z) + 2\sum_{m=1}^{P}\left[G_m^{n-1}e^{A_m\Delta t} - H_x^{n-\frac{1}{2}}\left(i,N_z-\frac{1}{2},k\right)\frac{C_m}{A_m}(e^{A_m\Delta t}-1)\right] \quad (35)$$

for the upper wall.

The piece linear equations can easily be constructed by modifying equations (32) through (35) keeping equation (29) in mind.

6. EFFECTS OF FDTD SIMULATION PARAMETERS ON IBC ACCURACY

In this section a numerical study of the effects of the FDTD simulation parameters such as grid spacing, time step, and the number of expansions terms is presented.

6.1 1D FDTD Simulation Configuration

Figure 3 is a representation of the 1D FDTD simulation set up used to analyze the effects of FDTD parameters on the IBC accuracy. An

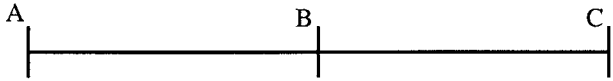

Figure 3. 1D configuration for IBC error analysis.

unmodulated Gaussian pulse is used to excite the problem at one end of the computational domain, point **A**, with the boundary condition $E_x^n(k=0) = g(n)$. The IBC is placed at point **B** and a first order Mur boundary condition is placed at the other end of the computational domain, point **C**. The propagation direction is z and a TEM wave, (E_x, H_y) is launched toward the IBC. The computational domain is 3000Δ long with **B** in the middle at $z = 1500\Delta$ or more simply $k = 1500$. The FDTD stability criteria for the time step is set to

$$\Delta t = \frac{\Delta}{CFL\, c}$$

where Δ is the spatial step size, c is the speed of light, and CFL is a real number that ensures that the Courant-Friedrichs-Lewy stability condition is satisfied. The normal 1D FDTD algorithm requires $CFL \geq 1$ for stability. Two simulations are run for any given test set up. The first simulation does not include the IBC at $k = 1500$. Instead the field is allowed to freely propagate to the right and the field is measured at $k = 1499$ and saved at all time steps to be used as the incident field when calculating the reflection coefficient of the IBC. The second simulation also measures the electric field at $k = 1499$; however this time, the IBC is in place at $k = 1500$. Here the stored field includes both the incident and reflected waves. By using this total field and the stored incident field the reflection coefficient is calculated up to 10 GHz. Even though the reflection coefficient would be a sufficient measure of the IBC, the transmissivity is calculated from the reflection coefficient via

$$t(f) = 10 \log[1 - |R(f)|^2]. \tag{36}$$

The transmissivity has the nice property that it increases with increasing frequency in this application.

Once the time step is determined by Δ and CFL, the frequency content of the incident pulse is controlled through the selection of β in

$$g(n\Delta t) = e^{-16(n\Delta t - \beta\Delta t)^2/(\beta\Delta t)^2}. \tag{37}$$

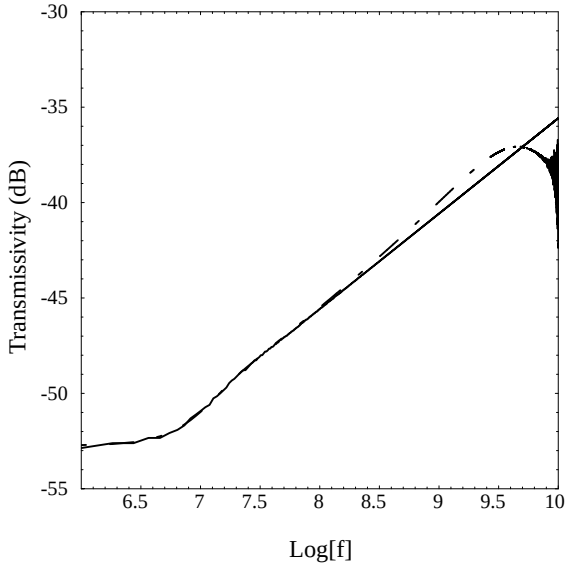

Figure 4. Transmissivity FDTD (dashed) vs. Analytic (solid) for a $35\,\mu$m thick sheet of copper with $\sigma = 5.8 \times 10^7\,\Omega^{-1}\mathrm{m}^{-1}$; $P = 20$, $\Delta = .005\,\mathrm{m}$, $CFL = 2.0$, and $\beta = 50$.

Figure 4 is a plot of the transmissivity measured from a $35\,\mu m$ thick sheet of copper with $\sigma = 5.8 \times 10^7\,\Omega^{-1}\mathrm{m}^{-1}$. The IBC is within 1 dB up to 3 GHz with only 20 expansion terms. In the next section the FDTD parameters are varied and the effects studied.

6.2 Transmissivity Error Measurements

The error analysis is based on a direct comparison between the FDTD transmissivity results versus the analytical transmissivity calculation using

$$e = \sqrt{\frac{\sum_{i=1}^{N}[t_a(f_i) - t_{FDTD}(f_i)]^2}{N}}, \tag{38}$$

where $t_{FDTD}(f_i)$ is the transmissivity calculated from the FDTD simulation and $t_a(f_i)$ is the equivalent analytical calculation at frequency, f_i.

The first FDTD parameter examined is the time step. The FDTD stability criteria requires $CFL \geq 1.0$. A larger time step can reduce

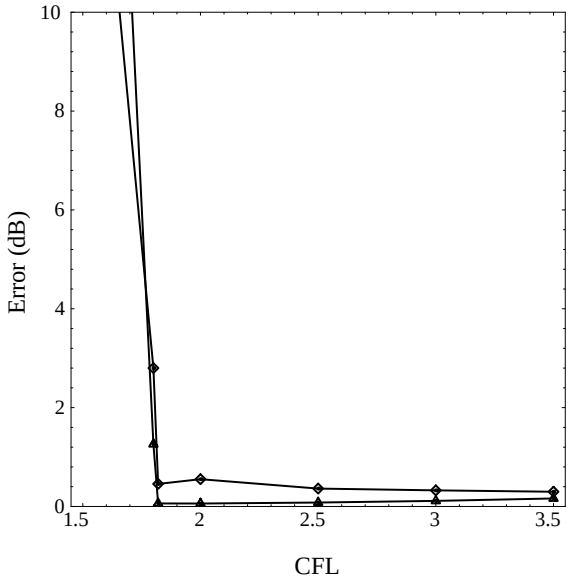

Figure 5. Error vs. CFL for a $35\,\mu$m thick conductor for two different FDTD configurations: (1) $\sigma = 5.8 \times 10^4\,\Omega^{-1}\mathrm{m}^{-1}$, $P = 3$, $\Delta = .005\,\mathrm{m}$ (diamond) and (2) $\sigma = 5.8 \times 10^7\,\Omega^{-1}\mathrm{m}^{-1}$, $P = 125$, $\Delta = .00125\,\mathrm{m}$ (triangle).

the run time and improve the frequency resolution in any post simulation processing. Typically, FDTD codes allow the users to set the grid spacing while the code automatically sets the time step at the Courant limit, so it's important to know if the IBC requires a time step smaller than the Courant stability limit in order to bound the error. Figure 5 shows the results from a numerical experiment with two very different simulation configurations. The conductivities are different, $5.8 \times 10^4\,\Omega^{-1}\mathrm{m}^{-1}$ versus $5.8 \times 10^7\,\Omega^{-1}\mathrm{m}^{-1}$; the number of expansion terms are different, $P = 3$ versus $P = 125$; and finally the grid spacing is different, $\Delta = .005\,\mathrm{m}$ versus $\Delta = .00125\,\mathrm{m}$. Both simulations used a sheet thickness of $35\,\mu$m and the β is adjusted at each simulation to ensure the same frequency content in the excitation. Also, all simulations were run for 8192 times steps and the Fourier transforms were taken with padding at 16 times the original length. The error is calculated with (38). The results show that in order to keep the error low the IBC definitely has a stricter time step constraint than the FDTD Courant stability limit. In fact, both 1D experimental configurations had the same CFL limit. The results

show that $CFL \geq 1.82$ is necessary to bound the error. This does not mean the algorithm is unstable when CFL is set to the Courant limit it just means the accuracy is very poor. Furthermore, it is important to note that the CFL is even larger than the 3D FDTD Courant limit of $\sqrt{3}$ for a uniform grid. Next the effects of grid size and number of expansion terms are studied. Figures 6 through 11 are plots of the transmissivity error of equation (38) versus the number of expansion terms at three different grid spacings, $\Delta = .005\,\mathrm{m}$, $\Delta/2$, and $\Delta/4$. All simulations used a conductor thickness of $35\,\mu\mathrm{m}$ and the β's were 50, 100, and 200 respectively. Figure 9 are the results with copper, $\sigma = 5.8 \times 10^7$, while Figures 6, 7, and 8, are the results for a conductivities three orders of magnitude less than copper and Figures 10 and 11 are the results for a conductivities 2 orders of magnitude greater than copper.

The results show the general trend that smaller grid size will reduce the error. This, of course, makes sense. The FDTD algorithm is more accurate with a smaller grid size. Also, the impedance in the FDTD IBC is approximated by electric and magnetic fields that are half a grid space apart, so the closer the grid space the more accurately the IBC scheme will approximate the actual impedance. However, the numerical results also show that the number of expansion terms plays a big role in the accuracy of the IBC algorithm and more terms does not necessarily mean more accuracy. For example, in Figure 6 we see that the error levels out at about 20 expansion terms. Interestingly, the optimum setting for P is about 5. Although the differences in error are less than $.2\,\mathrm{dB}$ and $.1\,\mathrm{dB}$ for $\Delta = .005\,\mathrm{m}$ and $\Delta = .00125\,\mathrm{m}$, respectively, these errors would accumulate in simulations where multiple reflections from the surface occur.

The optimum number of expansion terms is a function of conductivity and grid spacing. As Figure 9 indicates, the best values for P are approximately 50, 80, and 120 for a conductivity of $\sigma = 5.8 \times 10^7$ and a grid spacing of $\Delta = .005\,\mathrm{m}$, $\Delta = .0025\,\mathrm{m}$, and $\Delta = .00125\,\mathrm{m}$, respectively. Whereas for low and high conductivities the effect of grid spacing is much reduced.

The results clearly show that as the conductivity increases the number of terms needed to accurately approximate the impedance increases. In fact for the largest conductivity shown, $\sigma = 5.8 \times 10^9$, the IBC requires more than 250 terms to keep the error below $1\,\mathrm{dB}$.

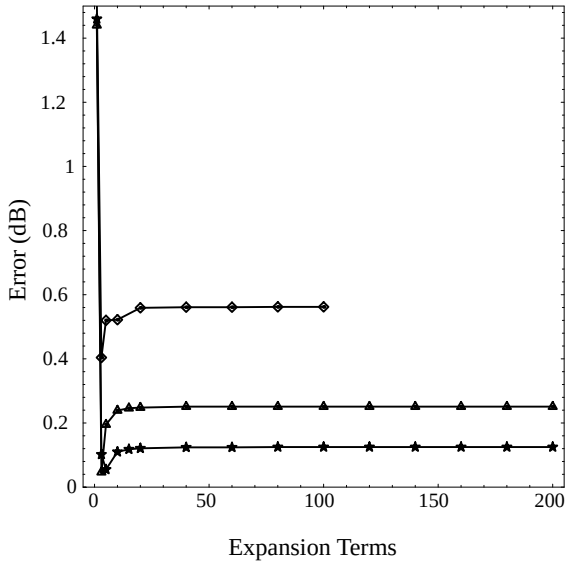

Figure 6. Error vs. expansion terms for a $35\,\mu$m thick conductor with $\sigma = 5.8\times10^4\,\Omega^{-1}\mathrm{m}^{-1}$; $\Delta = .005\,\mathrm{m}$ (diamond), $\Delta = .0025\,\mathrm{m}$ (triangle), $\Delta = .00125\,\mathrm{m}$ (star).

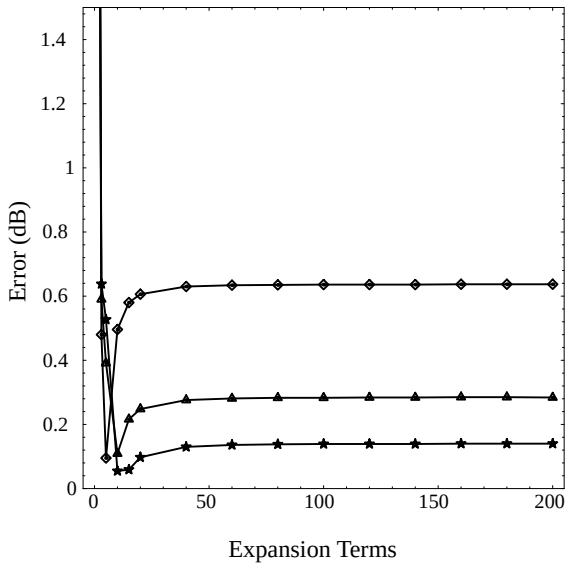

Figure 7. Error vs. expansion terms for a $35\,\mu$m thick conductor with $\sigma = 5.8\times10^5\,\Omega^{-1}\mathrm{m}^{-1}$; $\Delta = .005\,\mathrm{m}$ (diamond), $\Delta = .0025\,\mathrm{m}$ (triangle), $\Delta = .00125\,\mathrm{m}$ (star).

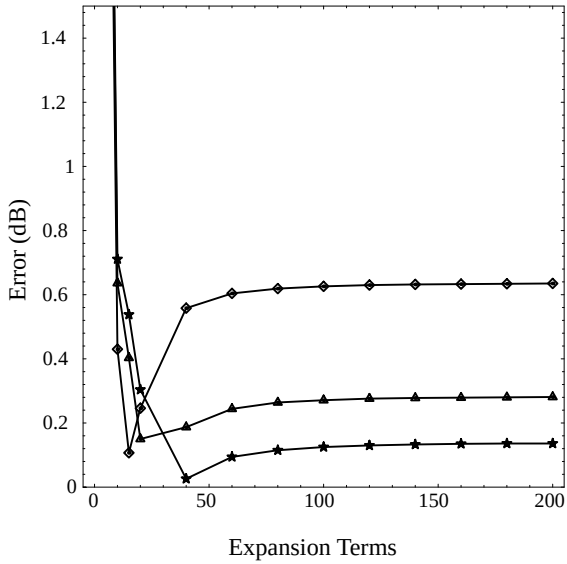

Figure 8. Error vs. expansion terms for a $35\,\mu$m thick conductor with $\sigma = 5.8 \times 10^6\,\Omega^{-1}\mathrm{m}^{-1}$; $\Delta = .005\,\mathrm{m}$ (diamond), $\Delta = .0025\,\mathrm{m}$ (triangle), $\Delta = .00125\,\mathrm{m}$ (star).

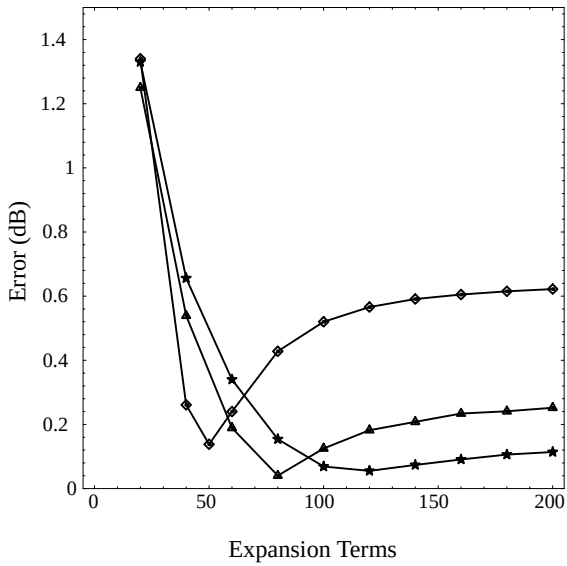

Figure 9. Error vs. expansion terms for a $35\,\mu$m thick conductor with $\sigma = 5.8\times10^7\,\Omega^{-1}\mathrm{m}^{-1}$; $\Delta = .005\,\mathrm{m}$ (diamond), $\Delta = .0025\,\mathrm{m}$ (triangle), $\Delta = .00125\,\mathrm{m}$ (star).

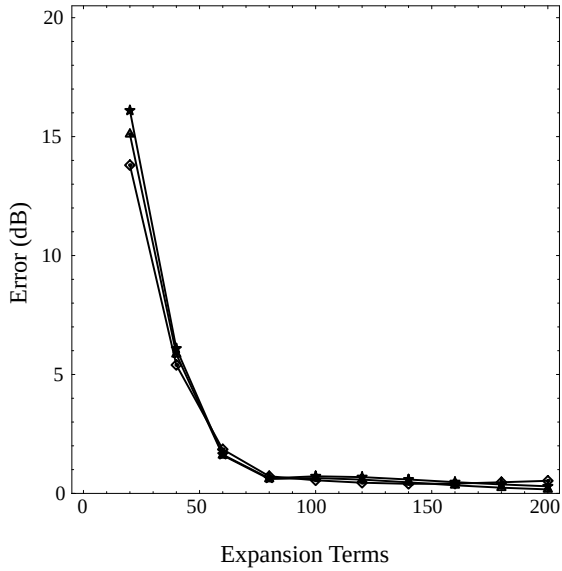

Figure 10. Error vs. expansion terms for a $35\,\mu$m thick conductor with $\sigma = 5.8 \times 10^8\,\Omega^{-1}\mathrm{m}^{-1}$; $\Delta = .005\,\mathrm{m}$ (diamond), $\Delta = .0025\,\mathrm{m}$ (triangle), $\Delta = .00125\,\mathrm{m}$ (star).

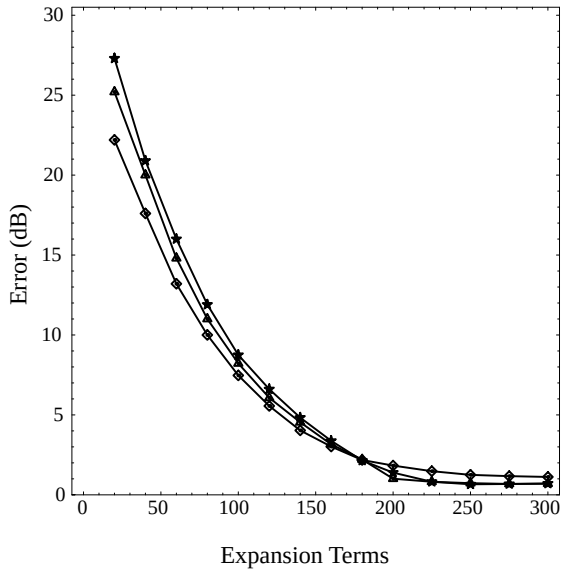

Figure 11. Error vs. expansion terms for a $35\,\mu$m thick conductor with $\sigma = 5.8 \times 10^9\,\Omega^{-1}\mathrm{m}^{-1}$; $\Delta = .005\,\mathrm{m}$ (diamond), $\Delta = .0025\,\mathrm{m}$ (triangle), $\Delta = .00125\,\mathrm{m}$ (star).

6.3 Optimum Settings

The fact that there is an *optimum* number of terms for the piecewise constant IBC seems to go against intuition. If additional terms more accurately model the impedance then why doesn't the error decrease as the number of expansion terms increase?

We begin with a look at the error results for the piecewise linear IBC for copper with $\sigma = 5.8 \times 10^7\,\Omega^{-1}\mathrm{m}^{-1}$ at three different grid spacings, as shown in Figure 12 versus the piecewise constant error in Figure 13. The two plots are combined in Figure 14. The results show that there is no optimum number of expansion terms (at least up to 300 terms) when using the piecewise linear IBC. Next, we look at the magnitude of main term in the piecewise constant IBC formulation, $e^{A_m \Delta t} - 1$, and plot it versus expansion number at the three time steps of Figure 12 as shown in Figure 15. Figure 15 shows that we should expect a leveling off of the error since the IBC term levels off rather quickly. Since the exponential term is proportional to the square of the expansion term number, it follows that the influence of the term will quickly decrease. Furthermore, the other factors in the exponential term should show similar results. As the conductivity decreases the number of strong influential terms decreases (Figures 6 through 11). As the conductor thickness increases the number of influential terms also increases (Figure 16).

There are essentially two approximations that contribute to the transmissivity error. The first is from the approximation of the impedance by a sum of exponentials, and the other is from the approximation to the convolution integral. The two convolution approximations used are piecewise constant and piecewise linear. When few expansion terms are used, the impedance error is the dominant error. As the number of terms increases, the impedance error decreases. If fact, it should approach zero as $m \to \infty$. Therefore, as m becomes sufficiently large, the convolution integral approximation error will dominate the overall error and increasing m will not improve the error. This is clearly evident in Figure 14 as seen by the leveling of the error curves at some small but finite error as m increases. The optimum settings evident in the piecewise constant must result from the combination of the two types of errors, and the piecewise linear error is evidently sufficiently small such that it does not produce an optimum setting.

Depending on the problem being considered, a non-optimum number of expansion terms may not lead to significant error since the errors

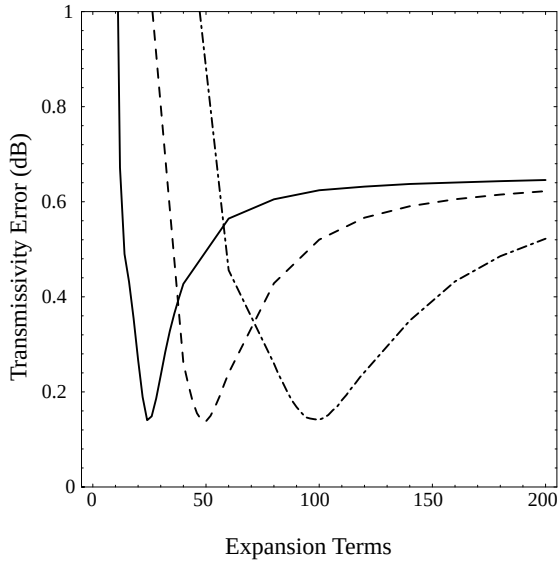

Figure 12. Piecewise linear error vs. expansion terms for a $35\,\mu$m thick conductor with $\sigma = 5.8 \times 10^7\,\Omega^{-1}\mathrm{m}^{-1}$; $\Delta = .005\,\mathrm{m}$ (solid), $\Delta = .0025\,\mathrm{m}$ (dash), $\Delta = .00125\,\mathrm{m}$ (dash-dot).

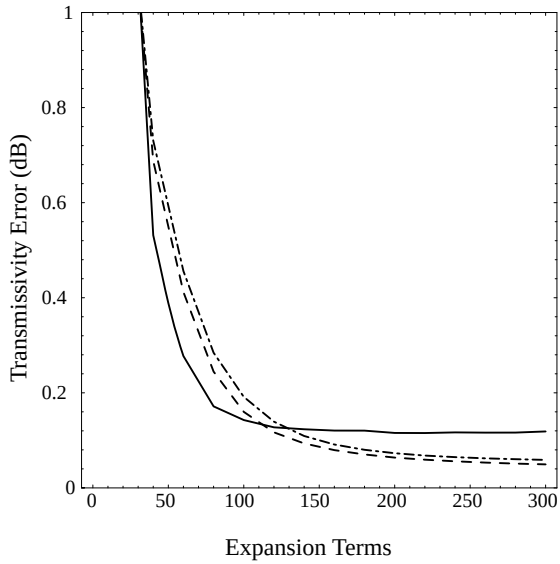

Figure 13. Piecewise constant error vs. expansion terms for a $35\,\mu$m thick conductor with $\sigma = 5.8 \times 10^7\,\Omega^{-1}\mathrm{m}^{-1}$; $\Delta = .005\,\mathrm{m}$ (solid), $\Delta = .0025\,\mathrm{m}$ (dash), $\Delta = .00125\,\mathrm{m}$ (dash-dot).

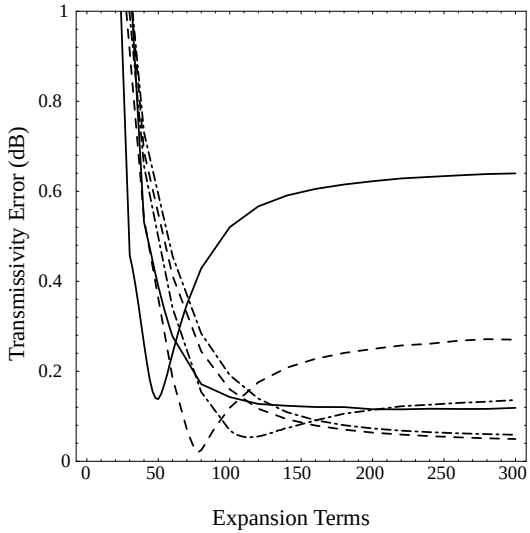

Figure 14. Comparison of error behavior of piecewise constant IBC and piecewise linear IBC for a $35\,\mu$m thick conductor with $\sigma = 5.8 \times 10^7\,\Omega^{-1}\mathrm{m}^{-1}$; $\Delta = .005\,\mathrm{m}$ (solid), $\Delta = .0025\,\mathrm{m}$ (dash), $\Delta = .00125\,\mathrm{m}$ (dash-dot).

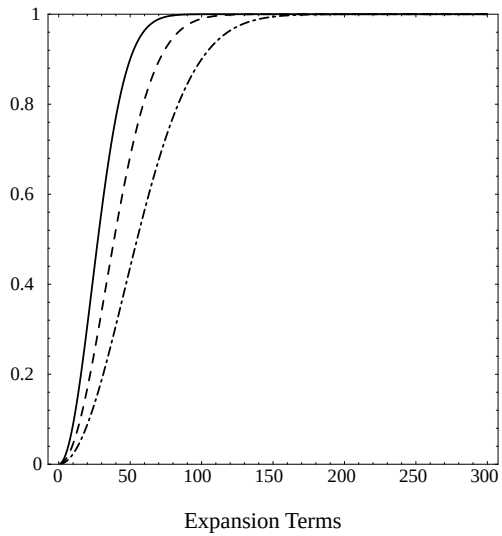

Figure 15. Magnitude of piecewise constant IBC term, $|e^{A_m \Delta t} - 1|$, vs. expansion terms for a $35\,\mu$m thick conductor with $\sigma = 5.8 \times 10^7\,\Omega^{-1}\mathrm{m}^{-1}$; $\Delta t = \frac{.005\,m}{2c}$ (solid), $\Delta t = \frac{.0025\,m}{2c}$ (dash), $\Delta t = \frac{.00125\,m}{2c}$ (dash-dot).

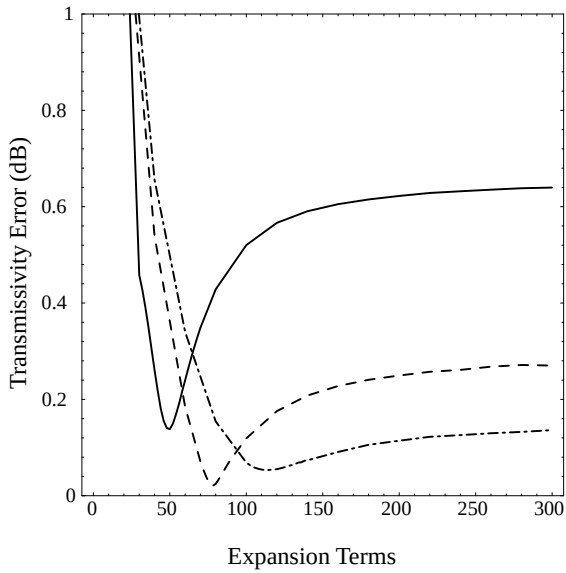

Figure 16. Piecewise constant error vs. expansion terms for various conductor thicknesses with $\Delta = .005\,\mathrm{m}$ and $\sigma = 5.8 \times 10^7\,\Omega^{-1}\,\mathrm{m}^{-1}$; $l = 17.5\,\mu\mathrm{m}$ (solid), $l = 35\,\mu\mathrm{m}$ (dash), $l = 70\,\mu\mathrm{m}$ (dash-dot).

are still small. However, if the problem includes many reflections from the IBC as in resonant cavities, the optimum number of terms should be considered when using the piecewise constant formulation.

7. VERIFICATION OF IBC IN TWO DIMENSIONS

Measurement of the quality factor of resonant structures is used to verify the multi-dimensional IBCs [9]. This method is desirable for two reasons. First, it is the very small but finite loss that a good conductor exhibits that causes errors in FDTD simulations where good conductors are represented by perfect conductors. Second, the measurement is based on many reflections from the cavity's surfaces and should give a good indication of the accuracy and thus the benefit of this type of IBC.

7.1 Calculation of Quality Factor

An analytical approximation for the quality factor of a resonant cavity is used for the comparison against the FDTD IBC. Using the

nomenclature and derivation found in [13], the essential ideas follow.

The quality factor of Q is a measure of the loss of a resonant cavity. Let $w_{T_n}(t)$ represent the total electromagnetic energy of a mode n within a resonant cavity. The energy can be approximated by

$$w_{T_n}(t) = w_{T_n}(0)e^{-\omega_n t/Q_n} \tag{39}$$

where w_n is the resonant frequency in radians of the n th mode. So using the definition in [13], the quality factor is the average number of radians it takes for the total electromagnetic energy to decay to $\frac{1}{e}$ of its original value. The higher the Q the lower the loss. The quality factor can be determine from the average power dissipated within the structure and the average electromagnetic energy stored within the structure given by

$$Q_n = \frac{\omega_n \times \text{energy stored in } n\text{th mode}}{\text{average power dissipated in } n\text{th mode}} = \frac{\omega_n w_{T_n}}{\langle P_n \rangle}. \tag{40}$$

The power lost in the resonant structures used in this article are a result of the current flowing through the walls of the cavity. So to calculate the Q of the resonant structure under test we must calculate the following two integrals:

$$w_{T_n} = \frac{1}{2}\int_V \epsilon_0 |\bar{E}_n|^2 dv \tag{41}$$

and

$$P_n = \frac{1}{2}\int_V \bar{E}_n \cdot \bar{J}_n^* dv. \tag{42}$$

As in [13], since we're dealing with very large conductivities perturbation methods can be used. The current can be approximated by the current generated in a perfect conductor. So the power calculation of (42) becomes

$$P_n \simeq \frac{1}{2}\int_V \frac{|\bar{J}_n^0|^2}{\sigma} dv, \tag{43}$$

where $\bar{J}_n^0$ represents the current in a resonator with PEC walls. Again using the *good* conductor approximation, most of the current flows within one skin depth of the conductor, where the skin depth, δ is defined by

$$\delta = \sqrt{\frac{2}{\omega_n \mu_0 \sigma}}, \tag{44}$$

and the current can be approximated by assuming that the current is equivalent to the surface current of a perfect conductor uniformly distributed over a single skin depth, so equation (43) becomes

$$P_n \simeq \frac{1}{2\sigma\delta} \int_A |\bar{J}^0_{sn}|^2 da, \tag{45}$$

where A is the inside surface of the resonator and $\bar{J}^0_{sn}$ is the surface current due to the nth mode in a PEC resonator. Figure 17 is a schematic of the test structure used to validate the two dimensional IBC. The test structure is a rectangular resonating cavity made with a good conductor with conductivity, σ, with dimensions (in meters) a in the x direction and c in the z direction. The thickness of the thin conducting sheet is l m and the skin depth is δ m. (The figure is not drawn to scale $l \ll a, c$.)

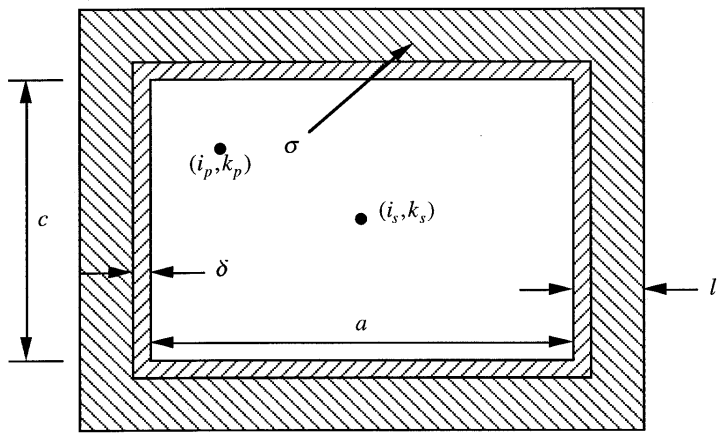

Figure 17. Test structure for IBC validation.

The cavity is excited with TE modes by using a line source located at (i_s, k_s) on a discretized FDTD grid and the response is measured with a software probe at (i_p, k_p) that records $E_y(i_p, k_p)$ at each time step.

For the power and energy calculations we assume infinite extent in the y direction and therefore the energy and power units are all described per meter.

With Figure 17 in mind the power dissipated per meter is given by

$$P_n = 2\frac{1}{2\sigma\delta}\int_0^a |\hat{z}\times\bar{H}_n^0(z=0)|^2 dx + 2\frac{1}{2\sigma\delta}\int_0^c |\hat{x}\times\bar{H}_n^0(x=0)|^2 dz. \quad (46)$$

Given a TE excitation (E_y), the mode can be described by

$$E_y(x,z) = E_o \sin k_x x \sin k_z z, \quad (47)$$

where $k_x = \frac{m\pi}{a}$, and $k_z = \frac{p\pi}{c}$. The magnetic fields can be found from Maxwell's equations and (47). They are

$$H_x(x,z) = i\frac{k_z}{\omega\mu_o} E_o \sin k_x x \cos k_z z \quad (48)$$

and

$$H_z(x,z) = -i\frac{k_x}{\omega\mu_0} E_o \cos k_x x \sin k_z z. \quad (49)$$

Using (48) and (49) in (46) the power becomes

$$\begin{aligned} P_{m,p} &= \frac{|E_0|^2}{2\sigma\delta\omega_{m,p}^2\mu_0^2}[ak_z^2 + ck_x^2] \\ &= \frac{|E_0|^2\pi^2}{2\sigma\delta\omega_{m,p}^2\mu_0^2 a^2c^2}[m^2a^3 + p^2c^3]. \end{aligned} \quad (50)$$

The total electromagnetic energy is calculated from (41) and (47), resulting in

$$w_{t_{m,p}} = \frac{ac}{8}\epsilon_0|E_0|^2. \quad (51)$$

Substitution of (50) and (51) into (40) yields

$$Q_{m,p} = \frac{\epsilon_0\sigma\delta\omega_{m,p}^3\mu_0^2 a^3c^3}{4\pi^2[m^2a^3 + p^2c^3]}, \quad (52)$$

substituting $\omega_{m,p}^2\epsilon_0\mu_0 = k_{m,p}^2 = k_x^2 + k_z^2 = \pi^2\left(\frac{1}{a^2} + \frac{1}{c^2}\right)$ we arrive at

$$Q_{m,p} = \frac{(a^2m^2 + c^2p^2)ac}{2\delta[m^2a^3 + p^2c^3]}. \quad (53)$$

The quality factor of a good conductor resonator is a function of the mode number, skin depth, and the physical dimensions of the resonator.

7.2 Measurement of Quality Factor in FDTD Simulations

There are two ways to measure the quality factor in a FDTD simulation. The first is the take the Fourier transform of the electric field measured by the software probe. By measuring the half-power bandwidth about the resonator's resonant frequencies, the quality factor can be derived [13, 14]. However, this method will require millions of time steps for very high Q structures. A more practical method relies on exciting a single mode and measuring the decay in the mode's field strength measured by the software probe. In the lossy resonator, the resonant frequencies are better described in the s domain, $s_{m,p} = -i\omega_{m,p} - \alpha_{m,p}$. Since the energy is proportional to the magnitude of the electric field squared, equation (39) can be rewritten as

$$w_{T_{m,p}}(t) = w_{T_{m,p}}(t=0)e^{-2\alpha_{m,p}t}, \tag{54}$$

and the quality factor becomes

$$Q_{m,p} = \frac{\omega_{m,p}}{2\alpha_{m,p}}. \tag{55}$$

If a single mode is excited in the FDTD simulation, $\alpha_{m,p}$ can be calculate from two peaks in the stored electric field, given by

$$\alpha_{m,p} = -\frac{\ln[E_y^{n_2}/E_y^{n_1}]}{(n_2 - n_1)\Delta t} \tag{56}$$

7.3 2D Simulations and Results

The impedance boundary condition is extended to two-dimensions. Using the test structure in Figure 17 the dimensions of the structure are changed to vary the frequency. The current source is placed at the center of the structure and the probe is off center. A modulated gaussian pulse, modulated at the $TE_{1,1}$ resonant frequency with $\beta = 4096$, is used as the temporal excitation. The software probe stores the electric field at each time step. Equation (56) is used to measure $\alpha_{1,1}$ and equation (55) is used to measure Q_{FDTD}. The simulated results

are compared to the analytically derived values of Q. Tables 1–4 show the results. Each table represents a different frequency and each table spans four orders of magnitude of conductivity. The tabular results are shown graphically in Figure 18.

Table 1. Comparison of Q_{FDTD} and analytic Q at 3.03 GHz.

MSiemans	l/δ	Q_{FDTD}	Q	% error
0.058	0.92	801.5	922.0	−13.1
0.58	2.92	2950.4	2915.5	+1.2
5.8	9.22	9220.3	9219.7	0.0
58.0	29.16	303657	29155.2	+3.8
580	92.20	100939.0	92196.8	+9.4

Table 2. Comparison of Q_{FDTD} and analytic Q at 6.06 GHz.

MSiemans	l/δ	Q_{FDTD}	Q	% error
0.058	1.30	693.5	652.0	+64
0.58	4.12	2019.6	2061.6	−2.0
5.8	13.04	6521.0	6519.3	0.0
58.0	41.23	20855.4	20615.8	+1.2
580	130.39	63140.3	65193.0	−3.1

Table 3. Comparison of Q_{FDTD} and analytic Q at 9.6 GHz.

MSiemans	l/δ	Q_{FDTD}	Q	% error
0.058	1.64	518.8	455.4	+13.9
0.58	5.18	1399.0	1440.2	−2.9
5.8	16.40	4574.4	4554.2	+0.4
58.0	51.85	14502.5	14401.7	+0.7
580	163.95	45889.3	45542.1	+0.8

Table 4. Comparison of Q_{FDTD} and analytic Q at 12.1 GHz.

MSiemans	l/δ	Q_{FDTD}	Q	% error
0.058	1.84	501.0	461.0	+8.7
0.58	5.83	1401.8	1457.8	−3.8
5.8	18.44	4642.0	4609.8	+0.7
58.0	58.31	14430.6	14577.6	−1.0
580	184.39	44324.1	46098.4	−3.8

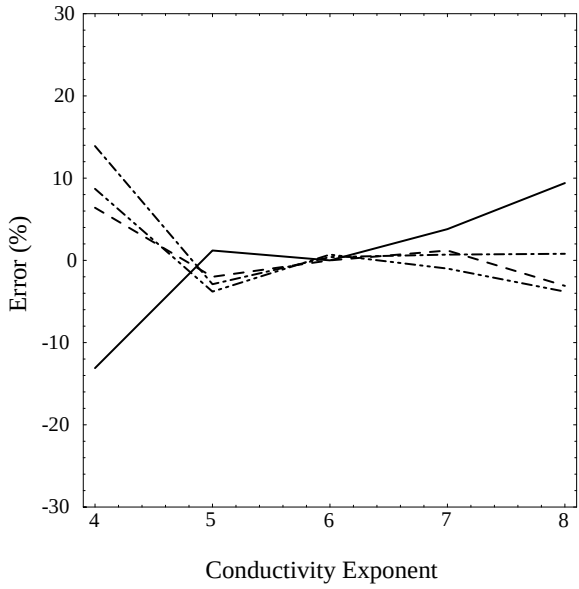

Figure 18. 2D resonator quality factor percent error versus conductivity exponent, x in $5.8 \times 10^x\,\Omega^{-1}\mathrm{m}^{-1}$; 3.03 GHz (solid), 6.06 GHz (dash), 9.60 GHz (dash-dot), 12.10 GHz (dash-dot-dot).

8. CONCLUSION

The conductivity range studied in this article spanned four orders of magnitude from 10^4 to $10^8\,\Omega^{-1}\mathrm{m}^{-1}$. (Some work at 10^9 was done in Section 6.2.) Even the lowest conductivity used would be considered a good conductor at the frequencies tested as defined by $1 \ll \frac{\sigma}{\omega\epsilon}$. The conductivities, in $\Omega^{-1}\mathrm{m}^{-1}$, of the most popular signal conductors, silver, copper, gold and aluminum are 6.14×10^7, 5.80×10^7, 4.10×10^7, and 3.54×10^7 and the conductivity of steel is 3.54×10^7 which all easily fall within the range of conductivities tested.

When a piecewise constant approximation is used for the magnetic field, the amount of computer resources (as measured by number of expansion terms) is directly proportional to the conductivity. Lower conductivities result in larger pole magnitudes and lesser sensitivity to increase number of terms. The piecewise constant approximation produces an error that cannot be overcome by more expansion terms. In fact, the errors from the impedance approximation and the magnetic field approximation combine to produce an optimum number of

expansion terms.

With a piecewise linear approximation, the error due to the magnetic field is greatly reduced and an optimum number of terms is not evident. The more terms used the more accurate the IBC; however, the error levels off at 200 terms in the test of the copper sheet in Section 6.3.

When extended to two dimensions, except for the lowest conductivity of $\sigma = 5.8 \times 10^4\,\Omega^{-1}\mathrm{m}^{-1}$ the impedance boundary condition works incredibly well over the wide range of skin depths studied, $3 \rightarrow 185$. The IBC is an excellent model for thin sheets of good conductors with finite conductivity. The IBC offers the advantage of working over a wide range of frequencies with very little computational overhead. For typical conductors, like copper, 125 terms per tangential electric field component are needed with errors in Q less than 5%.

REFERENCES

1. Choi, D. H. and W. J. R. Hoefer, "A graded mesh FD-TD algorithm for eigenvalue problems," *17th European Microwave Conference,* 413–417, 1987.
2. Kim, I. S. and W. J. R. Hoefer, "A local mesh refinement algorithm for the time domain-finite difference method using Maxwell's curl equations," *IEEE Trans. Microwave Theory Tech.,* Vol. 38, No. 6, 812–815, 1990.
3. Zivanovic, S. S., K. S. Yee, and K. K. Mei, "A subgridding method for the time-domain finite-difference method to solve Maxwell's equations," *IEEE Trans. Microwave Theory Tech.,* Vol. 39, No. 3, 471–479, 1991.
4. Beggs, J. H., R. J. Luebbers, K. S. Kunz, and K. S. Yee, "Wideband finite difference time domain implementation of surface impedance boundary conditions for good conductors," *IEEE Antennas and Propagat. Soc. Int. Symposium,* Vol. 1, 406–409, London, Ontario, 1991.
5. Lee, J.-F., R. Palandech, and R. Mittra, "Modeling three-dimensional discontinuities in waveguides using non-orthogonal FDTD algorithm," *IEEE Trans. Microwave Theory Tech.,* Vol. 40, No. 2, 346–352, 1992.
6. Wang, B. Z., "Time-domain modeling of the impedance boundary condition for an oblique incident parallel-polarization plane wave," *Microwave Opt. Technol. Lett.,* Vol. 7, No. 1, 19–22, 1994.
7. Oh, K. S. and J. E. Schutt-Aine, "An efficient implementation of surface impedance boundary conditions for the finite-difference

time-domain method," *IEEE Trans. Antennas Propagat.,* Vol. 43, No. 7, 660–666, 1995.

8. Luebbers, R. J., F. Hunsberger, K. S. Kunz, R. B. Standler, and M. Schneider, "A frequency-dependent finite-difference time-domain formulation for dispersive materials," *IEEE Trans. Electromagn. Compat.,* Vol. 32, No. 3, 222-227, 1990.
9. Chamberlin, K. and L. Gordon, "Deriving a synthetic conductivity to enable accurate prediction of losses in good conductors using FDTD," *10th Annual Review of Progress in Applied Computational Electromagnetics,* Vol. 2, 46–52, Monterey, CA, March 1994.
10. Lee, C. F., R. T. Shin, and J. A. Kong, "Time domain modeling of impedance boundary condition," *IEEE Trans. Microwave Theory Tech.,* Vol. 40, No. 9, 1847–1850, 1992.
11. Wang, B. Z., "Time-domain modeling of the impedance boundary condition for an oblique incident perpendicular-polarization plane wave," *Microwave Opt. Technol. Lett.,* Vol. 7, No. 8, 355–359, 1994.
12. Abramovitz, M. and I. A. Stegun, *Handbook of Mathematical Functions,* Dover Publications, New York, NY, 1965.
13. Staelin, D. H., J. A. Kong, and A. W. Morgenthaler, *Electromagnetic Waves,* Prentice Hall, Eaglewood Cliffs, NJ, 1994.
14. Johnson, D. E., J. L. Hilburn, and J. R. Johnson, *Basic Circuit Analysis,* Prentice-Hall, Eaglewood Cliffs, NJ, 1978.